Morphology Dependence of the Thermal Transport Properties of Single-Walled Carbon Nanotube Thin Films

S Yoshida[1], Y Feng[1], C Delacou[1], T Inoue[1], R Xiang[1], R Kometani[1], S Chiashi[1], E I Kauppinen[2] and S Maruyama[1, 3]

[1] Department of Mechanical Engineering, The University of Tokyo, 113-8656, Tokyo, Japan

[2] Department of Applied Physics, Aalto University School of Science, 15100, FI-00076 Aalto, Finland

[3] Energy NanoEngineering Laboratory, National Institute of Advanced Industrial Science and Technology (AIST), 305-8564, Tsukuba, Japan

E-mail: maruyama@photon.t.u-tokyo.ac.jp

Abstract. The thermal transport properties of random-network, single-walled carbon nanotube (SWNT) films were assessed using Raman spectroscopy. Two types of SWNT films were investigated: single-layer and stacked. The single-layer films were fabricated by aerosol chemical vapour deposition and subsequent direct dry-deposition, while the stacked films were prepared by placing the single-layer films on top of one another. The anisotropy of the network structures of each of these films was evaluated based on the angular dependence of the optical absorbance spectra. The results show that the anisotropy of the films decreases with increasing film thickness in the case of the single-layer films, and that the film anisotropy is preserved during the stacking process. The sheet thermal conductance is proportional to the SWNT area density in the case of stacked films, but is reduced with increasing thickness in the case of single-layer films. This effect is explained by a change in the network morphology from a two-dimensional anisotropic structure to the more isotropic structure. This work demonstrated the fabrication of low-density films with high sheet thermal conductance through the stacking of thin SWNT films.

PACS code: 44.10.+i

1. Introduction

Single-walled carbon nanotubes (SWNTs) [1] have received significant attention owing to their superior mechanical, electrical, optical and thermal properties [2]. Many research projects have been conducted with the aim of employing SWNTs in applications such as transistors [3], solar cells [4], and thermal interface materials [5]. The thermal transport properties of SWNTs are especially important because they may prevent the overheating of devices and, in some cases, can determine the

device performance. Thus, both enhancing and controlling the thermal transport properties of SWNTs are important with regard to their eventual industrial applications. Hone *et al.* and Pop *et al.* assessed the thermal conductivities of individual SWNTs and found values as high as 3000 W / m K [6,7]. However, it has also been reported that the thermal conductivity of individual SWNTs vary with length [8–11], diameter [12,13], chirality [14,15], and defects [16]. The thermal conductivities of vertically aligned SWNT films [17–19], and random-network SWNT films [20,21], have been shown to range from 1 to 100 W / m K. It is known that the thermal conductivity of SWNT ensembles such as these can be affected by phonon scattering [22–24], bundle structure [25], contact thermal resistance among the SWNTs [26] and other factors. Thus, in these ensembles of SWNTs, the superior thermal transport properties of individual SWNTs are not fully realized. On the other hand, the low thermal conductivity of SWNT film is advantageous for thermoelectric devices made of network of SWNTs [26,27]. The thermal transport properties of SWNT ensembles are still under investigation, and to date studies regarding the effects of the morphology of the SWNT network structure have been limited to computational simulations [25,28].

In the present work, we focused on the effects of the network structure of SWNTs on their thermal transport properties. Various random-network SWNT films were fabricated with different thicknesses, and their anisotropic morphologies were characterized based on the incident-angle dependence of their optical absorbance. The thermal transport properties of these SWNT films were assessed by Raman spectroscopy. We determined the sheet thermal conductance of the films, which is equivalent to the in-plane thermal conductance per unit film area, as well as the thermal conductivity of them. Based on the resulting data, the effects of film morphology on the thermal transport properties were examined. Finally, we produced low-density SWNT films with higher sheet thermal conductance by stacking thin films, thus demonstrating a novel but simple means of enhancing and tuning the sheet thermal conductance.

2. Experimental methods

2.1. Production process of the SWNT films

The SWNT films used in this study were synthesized by aerosol chemical vapour deposition (Aerosol CVD), in which the carbon source (CO) and catalyst nanoparticles were combined in the form of an aerosol, such that the SWNTs were synthesized in the resulting gas flow [29,30]. These SWNTs were deposited on nanoporous filter paper to form films with random network structures. This process is termed direct dry deposition [29,30], and allows the film thickness to be controlled by varying the deposition time. In addition, it is easy to transfer these films to other substrates. It should be noted that each of these films had the same chirality distribution. Six sample types were fabricated in preparation for the experimental trials: Films 1, 2, 3, 4, 1×2 and 1×3. Film 1, 2, 3 and 4 are termed single-layer films while Films 1×2 and 1×3 are referred to as stacked films. The thickness of each single-layer film was controlled by adjusting the deposition time, while the stacked films were obtained by stacking two and three sheets of Film 1, respectively. The stacking was performed by a wet transfer technique in which one film was fixed on another as a result of the surface tension of a liquid (water or ethanol), followed by evaporation of the liquid.

2.2. Measurement of the optical anisotropy

UV-vis-NIR spectrometer was employed to determine the optical absorbance of each film over the wavelength range of 400 to 3200 nm. The optical absorbance, A, was measured while changing the incident angle of P-polarized light, and can be expressed as

$$A = \varepsilon \rho_v L \tag{1}$$

where ε is the optical absorption coefficient and ρ_v is the density of the SWNTs, defined as the total length of SWNTs per unit volume. Here $L = L_0 / \cos\theta$ is the optical path length in the SWNT film,

where θ is the incident angle of the P-polarized light and L_0 is the thickness of the film. We estimated the anisotropy of the films by determining the angular dependence of the intensity of the E^S_{11} peak, corresponding to the first optical transition energy of the SWNTs, using the optical absorbance spectra.

2.3. Measurement of the thermal transport properties

To understand the thermal transport properties of these SWNT films, we defined a parameter termed the sheet thermal conductance, G_s, which represents the in-plane thermal conductance of a film per unit area. This value is analogous to electrical sheet conductance (inverse of sheet resistance) and is defined as

$$G_s = kL_0 \text{ [W / K sq]}, \tag{2}$$

where k is the thermal conductivity of the film. This parameter was employed because otherwise it is necessary to arbitrarily define the thickness of each SWNT film. Since these films have a fluffy morphology, the statistical error of the film thickness can be very large (as discussed later), and it is helpful to be able to compare the thermal transport properties without considering the accuracy of film thickness. Details about the film thickness measurement are described in the supplementary material.

Raman spectroscopy was used to assess the sheet thermal conductance of each film [31,32]. Originally, this method was applied to the determination of the thermal conductivity of graphene, although the thermal conductivities of SWNT films have been determined with similar techniques [20,33]. In this method, the thermal resistance of the film is calculated as

$$R_\text{m} = \frac{T_\text{m} - T_\text{a}}{Q}, \tag{3}$$

where Q is the energy of laser absorbed by the sample suspended over a hole, T_m is the temperature inside the laser spot, and T_a is the ambient temperature. Here, T_m is determined based on both the temperature dependence and the excitation laser power dependence of the G-band Raman spectra. In this study, the temperature dependence of the G-band peak position of each SWNT films was assessed while controlling the sample stage temperature and it was confirmed that the equation below is applicable to analysis of the data [34].

$$\omega(T) = \omega_0 - \frac{A_1}{\exp\left(A_2 \dfrac{\hbar\omega_0}{k_B T}\right) - 1}, \tag{4}$$

Here, $\hbar$ is Plank's constant, k_B is the Boltzmann constant, T is the sample temperature, $\omega_0 = 1594 \text{ cm}^{-1}$, $A_1 = 38.4 \text{ cm}^{-1}$ and $A_2 = 0.438$. An argon ion laser operating at $\lambda = 488$ nm was used for excitation, and the absorbed laser power was calculated based on the optical absorbance of the film. The sheet thermal conductance of each film was determined by inserting R_m [31] in the equation

$$G_\text{s} = \frac{\ln\left(\dfrac{R}{r}\right)}{2\pi(R_\text{m} - R_\text{c})}\beta, \tag{5}$$

where R is the radius of the hole on which the samples were suspended, r is the radius of the laser spot (300 nm) as determined using the edge of a silicon chip, R_c is the thermal contact resistance between the SWNT film and the substrate, and β is a constant determined by the geometry of the measurement system. The Raman measurements were conducted in a vacuum chamber at approximately 1 Pa, in which the temperature was controlled with a precision of $\pm$ 0.1 K. The films were suspended over copper substrates having a hole with a radius of 1.25 mm, through which a Gaussian laser beam was irradiated at the centre of the suspended sample. In the case of a sufficiently small sample, the results can be significantly affected by the contact thermal resistance. However, since the SWNT films were large compared to the radius of the laser spot, β can be set to 1 and R_c can be neglected [31]. The effects of convective heat transfer can also be neglected because of the vacuum environment, and the

effects of radiation are also regarded as small enough to be neglected. Finally, the temperature variations along the film thickness direction are negligible. Therefore, Eq. (5) is applicable to the SWNT films used in this work.

3. Results and discussion

3.1. Characterization of the SWNT films
Figure 1 (a) shows a scanning electron microscopy (SEM) image of Film 1, in which the in-plane random network structure of the SWNTs can be observed. Figure 1 (b) presents the Raman spectrum of Film 1, obtained using excitation with a λ = 488 nm laser at room temperature. The ratio of the G band to D band intensities indicates a very low defect concentration. The optical absorbance spectrum of Film 1 is presented in figure 1 (c), and shows characteristic SWNTs peaks: E^S_{11}, E^S_{22} and E^M_{11}. The E^S_{ii} and E^M_{ii} peaks are associated with the i-th optical transition energy of semiconducting and metallic SWNTs, respectively.

3.2. Optical anisotropy of the SWNT films
Figure 2 plots the relative intensities of E^S_{11} absorbance peaks as functions of the incident angle for the various SWNT films. The intensity values in this figure have been normalized by the peak intensity at θ = 0. In the case of anisotropic materials such as these films, ε will vary with the incident angle of light. To analyse the degree of anisotropy, the SWNTs were regarded as interconnected rigid bars, and the angular distribution of the bars was examined, where ϕ_i (- π / 2 $\leq \phi_i \leq \pi$ / 2) is the angle of bar i relative to the plane of incidence. To simplify our model, a probability density distribution, $p(\phi_i)$, was defined as

$$p(\phi_i) = \begin{cases} \dfrac{1}{2\phi_{max}} & \left(-\phi_{max} \leq \phi_i \leq \phi_{max}\right) \\[2em] 0 & \left(-\dfrac{\pi}{2} \leq \phi_i < -\phi_{max}, \ \phi_{max} < \phi_i \leq \dfrac{\pi}{2}\right) \end{cases}, \tag{6}$$

where ϕ_{max} is a constant (- π / 2 $\leq \phi_{max} \leq \pi$ / 2). Here, we also introduce an order parameter that indicates the anisotropy of the films:

$$S(\phi_{max}) = 2\left\langle \cos^2 \phi_{ij} \right\rangle - 1 = \frac{\sin 2\phi_{max}}{2\phi_{max}}, \tag{7}$$

where ϕ_{ij} is the angle between two bars in the plane of incidence. A result of S ($\phi_{max} = \pi$ / 2) = 0 indicates that the film has a perfect isotropic network structure, while S (ϕ_{max} = 0) = 1 means that the film has an anisotropic structure, based on confining all the SWNTs within a two-dimensional (2D) plane. If the incident angle of light is θ, the optical absorption coefficient, ε, can be expressed as

$$\varepsilon(\theta, S(\phi_{max})) = \frac{1}{2\phi_{max}} \int_{-\phi_{max}}^{\phi_{max}} a_0 \cos^2 (\phi_i + \theta) d\phi_i = \frac{a_0}{2} \left[1 + \frac{\sin 2\phi_{max}}{2\phi_{max}} \cos 2\theta \right], \tag{8}$$

where a_0 is the optical absorbance of a unit SWNT length when the polarization of the incident light is parallel to the SWNT axis. It should be noted that variation of the optical anisotropy of individual SWNTs with $\cos 2\theta$ has been confirmed experimentally [35]. Thus, the optical absorbance for a SWNT film, A, depends on both S and θ. The θ dependence of A (S (ϕ_{max})) is

$$\frac{A(\theta, S(\phi_{max}))}{A(\theta = 0, S(\phi_{max}))} = \frac{\varepsilon(\theta, S(\phi_{max}))}{\varepsilon(\theta = 0, S(\phi_{max}))} \frac{\rho \frac{L_0}{\cos\theta}}{\rho L_0} = \frac{1 + \frac{\sin 2\phi_{max}}{2\phi_{max}}\cos 2\theta}{\left(1 + \frac{\sin 2\phi_{max}}{2\phi_{max}}\right)\cos\theta}, \tag{9}$$

Using the values of S, the normalized area density of the SWNTs, ρ_s / ρ_s^*, in each film could be obtained using the equation

$$\frac{A(\theta, S)/\varepsilon(\theta, S)}{A(\theta = 0, S^*)/\varepsilon(\theta = 0, S^*)} = \frac{\rho_s}{\rho_s^*}, \tag{10}$$

Here, the asterisk indicates the value obtained for Film 1. In these calculations, we defined the area density, ρ_s, as the total SWNT length per unit area, such that $\rho_s = \rho_v L_0$. The present data were fitted with Eq. (9) and the fits are shown in figure 2. Table 1 summarizes the film thickness values, L_0, as measured using an optical profiler (supplementary figure S5), optical absorbance, A (at $\theta = 0$) at $\lambda = 550$ nm, ρ_s / ρ_s^* values, order parameters, S, sheet electrical conductance, G_{el}, as measured by four-point probe method, thermal conductivities, k of the films and sheet thermal conductance G_s (as discussed further on).

Table 1. Data obtained for the SWNT films.

Film name	L_0 [nm]	A ($\theta = 0$)	ρ_s / ρ_s^*	S	G_{el} [mS m]	k [W / m K]	G_s [μW / K]
Film 1	62.6 ± 16.6	0.1286647	1	0.94	3.285	25.4 ± 7.01	1.59 ± 0.116
Film 2	62.8 ± 18.3	0.2044934	1.60	0.75	4.548	33.9 ± 9.87	2.13 ±0.141
Film 3	70.5 ± 18.5	0.4523918	4.70	0.58	9.091	73.7 ± 19.3	5.19 ± 0.627
Film 4	86.9 ± 20.7	0.5841665	6.08	0.43	13.98	69.6 ± 17.0	6.18 ± 0.490
Film 1×2	77.8 ± 16.9	0.2078240	2.44	0.94	-	50.5 ± 14.6	3.93 ± 0.279
Film 1×3	118 ± 25.8	0.3088104	4.21	0.94	-	64.0 ± 11.8	7.55 ± 1.11

These data confirm that the absorbance peak intensity decreased with increases in the incident angle of light, and that the anisotropy of each normal film (Films 1, 2, 3 and 4) increased with decreasing film thickness. Furthermore, the two stacked films (Films 1×2 and 1×3) followed the same trend as the normal Film 1. This result indicates that the anisotropy of each SWNT film was preserved during the film stacking process. In addition, it appears that the thinnest single-layer film (Film 1) and the stacked films all had anisotropic network structures (S approximately equal to 1), while the thicker single-layer films (Films 2, 3 and 4) had less anisotropic network structures (with small S values). These effects resulted from the dry deposition process, during which the SWNTs were more likely to form more isotropic networks with increasing film thickness. In addition, it was observed that the electrical sheet thermal conductance increases with increasing the thickness as confirmed in the previous study [29].

3.3. Thermal transport properties of the SWNT films

Figure 3 summarizes the relationship between absorbed laser power and the temperature rise inside the laser spot during Raman spectroscopy, and also includes fits based on Eq. (3). The linear relationship evident in this figure implies the validity of the approximation in Eq. (5), as discussed above. The slope of the fit is equal to the thermal resistance of the films, R_m, so the sheet thermal conductance, G_s, can be calculated using Eq. (5). Note that the measurement model provides the sheet thermal conductance of SWNT films averaged over suspended area (1.25 mm radius), and the SWNT films can be regarded as spatially uniform at this scale. The thermal conductivity of the films, k, can also be obtained by combining Eqs. (2) and (5). Although k should not depend on the thickness, L_0, in the case of bulk materials, the k values of the stacked films with the same S value tend to increase with

increasing L_0, which is due to an increase in percolation pathways with L_0 [36]. Thus, it is expected that k of SWNT films varies depending on L_0 and saturates if L_0 is sufficiently large. In the previous studies, it is reported that k of randomly-oriented SWNT films was determined to be 25 W / m K by using the opto-thermal technique when L_0 is 50 nm [20] while k was determined to be 80 W / m K by using infrared thermal imaging when L_0 was $400 - 500$ nm [21]. The resulting k values, presented in table 1, are comparable to those of the previous studies.

3.4. Morphology dependence of the sheet thermal conductance
Figure 4 shows the relationship between ρ_s / ρ_s^* and G_s. If each individual SWNT works as a heat conduction pathway, G_s should be proportional to the SWNT area density. The red line in figure 4 is the fit for the data obtained from Film 1 and the two stacked films, and indicates that their G_s values increase in proportion to the increasing number of heat conduction pathways (equivalent to the area density). In contrast, the thicker normal films (Films 2, 3 and 4) deviate to the lower side of the line, meaning that a simple increase in the amount of SWNTs in a film does not always contribute to an increase in G_s. These results suggest that the degree of isotropy of a film increases the out-of-plane heat conduction, which does not contribute to the in-plane heat conduction, G_s. The effect of anisotropy on G_s is remarkable. In the case of Film 4, which possesses relatively isotropic morphology, G_s decreases by about 40 % from the estimated value for anisotropic films with the same area SWNT density. The present results show that random-network SWNT films exhibiting arbitrary sheet thermal conductance can be fabricated with the minimum amount of SWNTs by stacking anisotropic 2D (S = 1) network structure films. Additionally, it is proposed that the area density and anisotropy of SWNT films should be carefully controlled to obtain the required thermal conductance depending on the application.

4. Conclusion
In conclusion, we measured the anisotropy of SWNT films made by aerosol CVD. The anisotropy increased with decreasing film thickness and was preserved when the films were stacked. The sheet thermal conductance of these SWNT films were determined by Raman spectroscopy. While the sheet thermal conductance of stacked films (S approximately 1) were proportional to the area densities of the SWNTs, more isotropic films (with lower S values) exhibited lower sheet thermal conductance, indicating that the sheet thermal conductance of a film depends significantly on the morphology of the SWNTs. Finally, we were able to obtain lighter SWNT films with higher sheet thermal conductance by stacking anisotropic 2D ($S = 1$) network structure films.

References
[1]   Iijima S and Ichihashi T 1993 Single-shell carbon nanotubes of 1-nm diameter *Nature* **363** 603–5
[2]   Saito R, Dresselhaus G and Dresselhaus M S 1998 *Physical Properties of Carbon Nanotubes* (London: Imperial College Press)
[3]   Brady G J, Way A J, Safron N S, Evensen H T, Gopalan P and Arnold M S 2016 Quasi-ballistic carbon nanotube array transistors with current density exceeding Si and GaAs *Sci. Adv.*

2 1–9

[4]   Jeon I, Chiba T, Delacou C, Guo Y, Kaskela A, Reynaud O, Kauppinen E I, Maruyama S and Matsuo Y 2015 Single-Walled Carbon Nanotube Film as Electrode in Indium-Free Planar Heterojunction Perovskite Solar Cells: Investigation of Electron-Blocking Layers and Dopants *Nano Lett.* **15** 6665–71

[5]   Panzer M A, Duong H M, Okawa J, Shiomi J, Wardle B L, Maruyama S and Goodson K E 2010 Temperature-dependent phonon conduction and nanotube engagement in metalized single wall carbon nanotube films *Nano Lett.* **10** 2395–400

[6]   Hone J, Whitney M, Piskoti C and Zettl A 1999 Thermal conductivity of single-walled carbon nanotubes *Phys. Rev. B* **103** 2498–9

[7]   Eric P, David M, Qian W, Kenneth G and Hongjie D 2006 Thermal Conductance of an Individual Single-Wall Carbon Nanotube above Room Temperature *Nano Lett.* **6** 96

[8]   Maruyama S 2002 A molecular dynamics simulation of heat conduction in finite length SWNTs *Phys. B* **323** 193–5

[9]   Mingo N and Broido D A 2005 Length Dependence of Carbon Nanotube Thermal Conductivity and the " Problem of Long Waves " *Nano Lett.* **5** 1221–5

[10]   Wang Z L, Tang D W, Li X B, Zheng X H, Zhang W G, Zheng L X, Zhu Y T, Jin A Z, Yang H F and Gu C Z 2007 Length-dependent thermal conductivity of an individual single-wall carbon nanotube *Appl. Phys. Lett.* **91** 4–7

[11]   Yamamoto T, Konabe S, Shiomi J and Maruyama S 2009 Crossover from ballistic to diffusive thermal transport in carbon nanotubes *Appl. Phys. Express* **2** 95003

[12]   Fujii M, Zhang X, Xie H, Ago H, Takahashi K, Ikuta T, Abe H and Shimizu T 2005 Measuring the thermal conductivity of a single carbon nanotube *Phys. Rev. Lett.* **95** 8–11

[13]   Lindsay L, Broido D A and Mingo N 2010 Diameter dependence of carbon nanotube thermal conductivity and extension to the graphene limit *Phys. Rev. B* **82** 161402

[14]   Zhang G and Li B 2005 Thermal conductivity of nanotubes revisited: Effects of chirality, isotope impurity, tube length, and temperature *J. Chem. Phys.* **123** 114714

[15]   Zhu L and Li B 2014 Low thermal conductivity in ultrathin carbon nanotube (2, 1). *Sci. Rep.* **4** 4917

[16]   Bifano M F P, Park J, Kaul P B, Roy A K and Prakash V 2012 Effects of heat treatment and contact resistance on the thermal conductivity of individual multiwalled carbon nanotubes using a Wollaston wire thermal probe *J. Appl. Phys.* **111** 54321

[17]   Hu X J, Padilla A a., Xu J, Fisher T S and Goodson K E 2006 3-Omega Measurements of Vertically Oriented Carbon Nanotubes on Silicon *J. Heat Transfer* **128** 1109

[18]   Shaikh S, Li L, Lafdi K and Huie J 2007 Thermal conductivity of an aligned carbon nanotube array *Carbon N. Y.* **45** 2608–13

[19]   Akoshima M, Hata K, Futaba D N, Mizuno K, Baba T and Yumura M 2009 Thermal diffusivity of single-walled carbon nanotube forest measured by laser flash method *Jpn. J. Appl. Phys.* **48** 05EC07

[20]   Duzynska A, Taube A, Korona K P, Judek J and Zdrojek M 2015 Temperature-dependent thermal properties of single-walled carbon nanotube thin films *Appl. Phys. Lett.* **106** 183108

[21]   Lian F, Llinas J P, Li Z, Estrada D and Pop E 2016 Thermal conductivity of chirality-sorted carbon nanotube networks *Appl. Phys. Lett.* **108** 103101

[22]   De Martino A, Egger R and Gogolin A O 2009 Phonon-phonon interactions and phonon damping in carbon nanotubes *Phys. Rev. B* **79** 1–14

[23]   Aliev A E, Lima M H, Silverman E M and Baughman R H 2010 Thermal conductivity of multi-walled carbon nanotube sheets: radiation losses and quenching of phonon modes. *Nanotechnology* **21** 35709

[24]   Hida S, Hori T, Shiga T, Elliott J and Shiomi J 2013 Thermal resistance and phonon scattering at the interface between carbon nanotube and amorphous polyethylene *Int. J. Heat Mass Transf.* **67** 1024–9

[25]   Duong H M, Yamamoto N, Bui K, Papavassiliou D V., Maruyama S and Wardle B L 2015 Morphology effects on non-isotropic thermal conduction of aligned single- and multi-walled carbon nanotubes in polymer nanocomposites *J. Phys. Chem. C* **114** 8851–60

[26]   Fukumaru T, Fujigaya T and Nakashima N 2015 Development of n-type cobaltocene-encapsulated carbon nanotubes with remarkable thermoelectric property. *Sci. Rep.* **5** 7951

[27]   Avery A D, Zhou B H, Lee J, Lee E-S, Miller E M, Ihly R, Wesenberg D, Mistry K S, Guillot S L, Zink B L, Kim Y-H, Blackburn J L and Ferguson A J 2016 Tailored semiconducting carbon nanotube networks with enhanced thermoelectric properties *Nat. Energy* **1** 16033

[28]   Volkov A N and Zhigilei L V. 2012 Heat conduction in carbon nanotube materials: Strong effect of intrinsic thermal conductivity of carbon nanotubes *Appl. Phys. Lett.* **101** 3–7

[29]   Kaskela A, Nasibulin A G, Timmermans M Y, Aitchison B, Papadimitratos A, Tian Y, Zhu Z, Jiang H, Brown D P, Zakhidov A and Kauppinen E I 2010 Aerosol-Synthesized SWCNT Networks with Tunable Conductivity and Transparency by a Dry Transfer Technique *Nano Lett.* **10** 4349–55

[30]   Nasibulin A G, Kaskela A, Mustonen K, Anisimov A S, Ruiz V, Rackauskas S, Timmermans M Y, Pudas M and Aitchison B 2011 Multifunctional Free-Standing Single-Walled Carbon Nanotube Films *ACS Nano* **5** 3214–21

[31]   Cai W, Moore A L, Zhu Y, Li X, Chen S, Shi L and Ruoff R S 2010 Thermal transport in suspended and supported monolayer graphene grown by chemical vapor deposition *Nano Lett.* **10** 1645–51

[32]   Chen S, Moore A L, Cai W, Suk J W, An J, Mishra C, Amos C, Magnuson C W, Kang J, Shi L and Ruoff R S 2011 Raman measurements of thermal transport in suspended monolayer graphene of variable sizes in vacuum and gaseous environments *ACS Nano* **5** 321–8

[33]   Sahoo S, Chitturi V R, Agarwal R, Jiang J and Katiyar R S 2014 Thermal Conductivity of Freestanding Single Wall Carbon Nanotube Sheet by Raman Spectroscopy *ACS Appl. Mater. Interfaces* **6** 19958–65

[34]   Chiashi S, Murakami Y, Miyauchi Y and Maruyama S 2008 Temperature dependence of raman scattering from single-walled carbon nanotubes: undefined radial breathing mode peaks at high temperatures *Jpn. J. Appl. Phys.* **47** 2010–5

[35]   Ichida M, Mizuno S, Kataura H, Achiba Y and Nakamura A 2004 Anisotropic optical properties of mechanically aligned single-walled carbon nanotubes in polymer *Appl. Phys. a-Materials Sci. Process.* **78** 1117–20

[36]   Volkov A N and Zhigilei L V. 2010 Scaling laws and mesoscopic modeling of thermal conductivity in carbon nanotube materials *Phys. Rev. Lett.* **104** 3–6
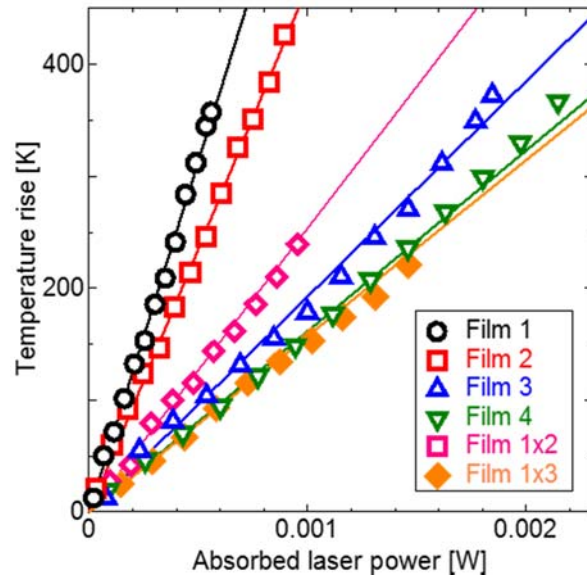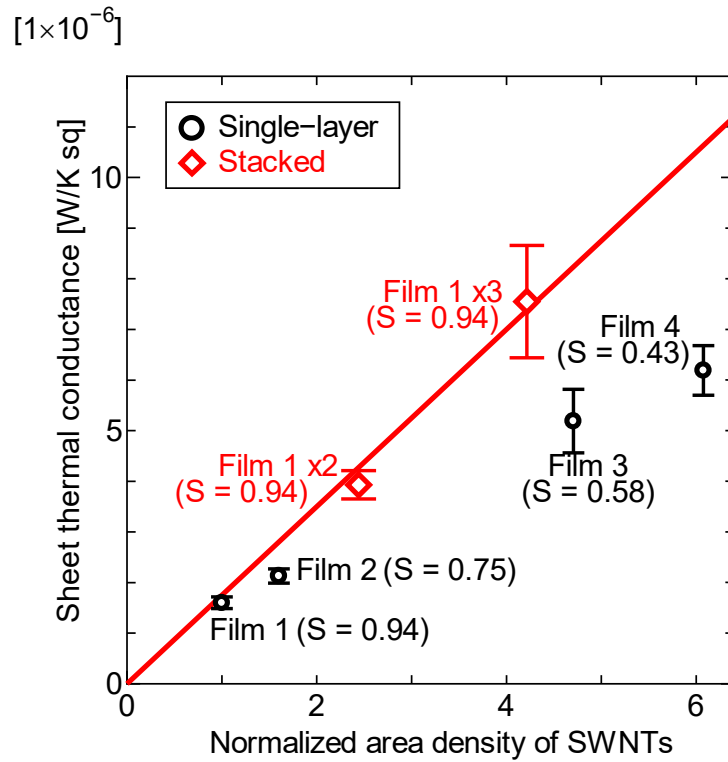
Figures
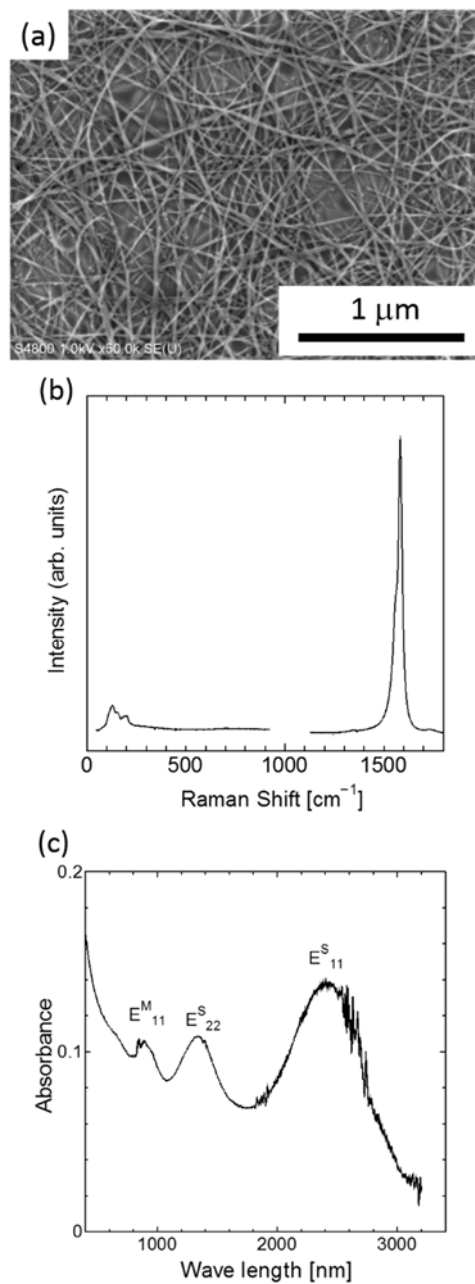
Figure 1. (a) SEM image of Film 1, in which the random network structure of the SWNTs can be seen, (b) Raman scattering spectrum of a SWNT film, with a G / D ratio > 100, in which RBM peaks are seen in the low frequency region, and (c) optical absorbance spectrum of a SWNT films. Here, E^S_{11}, E^S_{22} and E^M_{11} indicate the absorption peaks associated with each transition energy between van Hove singularities.
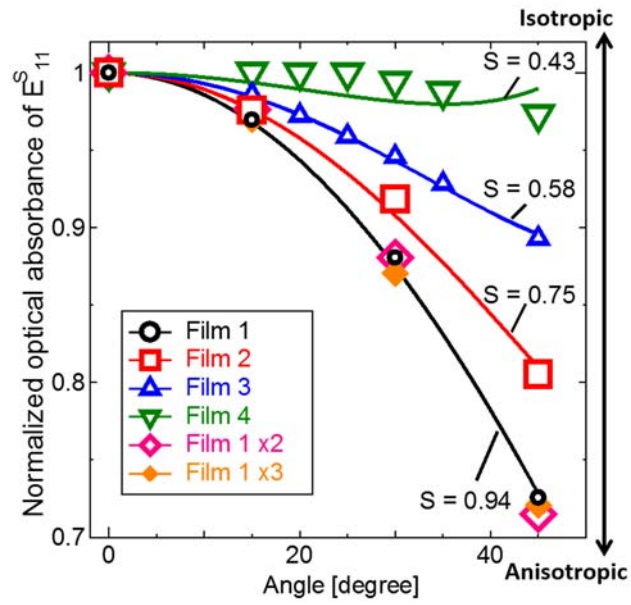
Figure 2. Relationship between the incident angle and the normalized optical absorbance of SWNT films for the E^S_{11} peak. The solid lines are fitted curves using Eq. (9), and the S values of each film are shown. The absorbance was normalized by that at an incident angle $\theta = 0$ for each SWNT film.

Figure 3. Relationship between absorbed laser power and the temperature rise inside the laser spot. The solid lines are fits obtained using Eq. (3). The values on the horizontal axis were calculated based on the optical absorbance values in table 1.

Figure 4. Relationship between normalized area density and sheet thermal conductance. The red solid line is the fit for Film 1 and the stacked films. While the stacked films show an ideal linear relationship, the thicker normal films deviate to lower conductance.